scientific reports

Check for updates

OPEN

# Biosynthesis, characterization and anthelmintic activity of silver nanoparticles of *Clerodendrum infortunatum* isolate

Rima Majumdar & Pradip Kumar Kar✉

**Over the past few decades, the green synthesis of nanoparticles has gained importance for their therapeutic efficacy and eco-friendly nature. Integrating green chemistry principles into multidisciplinary nanoscience research has paved the way for developing environmentally benign and sustainable methods for synthesizing gold and silver nanoparticles. In the present study, the flowers obtained from *Clerodendrum infortunatum* (L.), belonging to the family Verbenaceae, have been used for biosynthesizing silver nanoparticles (AgNPs) to evaluate the anthelmintic potential. UV–Vis spectroscopy, XRD, FTIR, SEM and TEM analyses were performed to ascertain the formation of AgNPs. Clerodendrum-derived AgNP (CLE-AgNP) has significantly affected the normal physiological functions of the poultry parasite *Raillietina* spp., a menace to the livestock industry. Our study manifests that CLE-AgNPs cause considerable distortion of the surface tegument of this cestode parasite leading to changes in the host-parasite interface. The histochemical localization studies of the tegument-associated enzymes viz. AcPase, AlkPase, ATPase and 5′-Nu, exposed to the drug, showed a substantial activity decline, thus establishing the anthelmintic potential of the CLE-AgNPs.**

Current trends in animal welfare boost the adoption of organic, pen-free range, and backyard husbandry practices. Local chicken managed under the backyard poultry production sector is critical in providing income for small societies. However, the growth of this sector is greatly hampered by the re-emergence of a diverse array of poultry helminths. Several studies suggest chickens and turkeys serve as hosts to a wide range of helminths, causing a huge economic loss in tropical countries like India. The cestode parasite *Raillietina* spp. is highly prevalent in common domestic fowl *Gallus gallus domesticus*, causing enteritis and weight loss in young chickens[1,2]. Common parasite eradication strategies include using the benzimidazole class of compounds, such as flubendazole, fenbendazole, and albendazole, whose unregulated usage can lead to antihelmintic resistance[3]. Although ethnoveterinary medicine is a well-established practice, evidence on the pharmacology of plant anthelmintics for use in chickens is limited. The current investigation has been conducted to support the therapeutic use of *Clerodendrum infortunatum* (CLE) for the biosynthesis of AgNP as an anthelmintic against the bird cestode *Raillietina* spp.

Bioinspired technology for nanoparticle (NP) synthesis has become a major branch within nanoscience and nanotechnology. So far, numerous metal NPs and metal oxides have been synthesized using plant extracts, microbes, etc[4,5]. Due to their wide availability, renewability, and environmental friendliness, in addition to their immense applications in the synthesis of NPs, plant biomass is mostly targeted as a catalyst for chemical synthesis and biodiesel production[6,7]. Silver products have long been known to have strong inhibitory and bactericidal effects and a broad spectrum of antimicrobial activities, which have been used for centuries to prevent and treat various diseases, most notably infections[8]. Current research suggests that silver nanoparticles (AgNPs) can be used in various medical applications, including antibacterial, antifungal, anti-diabetic, anti-inflammatory, and cancer treatment, as well as diagnosis[9–12]. The synthesis of silver nanoparticles by physical and chemical routes poses serious problems like high capital investment, usage of hazardous chemicals, high temperature and pressure, and toxic solvents[13–15]. Compared to microorganisms, applying plant extracts to synthesize AgNPs is more advantageous in resource availability, security, reaction rate and convenience, and feasibility of large-scale synthesis[16–18]. The phytochemicals present in plant extracts have been reported to cause the reduction of metal ions to nanoparticles and eventually obliterate the use of toxic chemicals, high pressure, temperature, energy

Parasitology Laboratory, Department of Zoology, Cooch Behar Panchanan Barma University, Vivekananda Street, Cooch Behar 736101, West Bengal, India. ✉email: karpradip@gmail.com

and maintenance of microbial cultures[19–24]. Various plant materials, such as leaf extracts, fruit, bark, fruit peels, root and callus, have been explored to synthesize NPs in different sizes and shapes[25]. Tripathi et al. evaluated the bactericidal activity of silver nanoballs at a concentration of 40 µg/mL against *Escherichia coli*, *Salmonella typhimurium*, *Bacillus subtilis*, and *Pseudomonas aeruginosa* by measuring colony-forming units[26]. In a previous study, Kar et al. investigated the in vitro anthelmintic activity of the nanogold particles synthesized by mycelia-free culture filtrate of the fungus *Nigrospora oryzae* treated with gold chloride on worm parasites using a cestode (tapeworm) model[27]. The study revealed alterations in the enzyme activity and effect on the normal physiological functioning of the parasite after treatment with gold nanoparticles.

In this research work, we focus on the bio-augmented synthesis of AgNPs using an aqueous extract of medicinally important CLE. Clerodendrum is a genus of flowering plants in the Lamiaceae (Verbenaceae) family that is very common throughout the plains of India, found widely in West Bengal. Although above 400 species of the genus, Clerodendrums are distributed worldwide, only a few have been investigated and studied so far[28]. Plants belonging to the genus Clerodendrum are well known for their pesticidal properties, and various Clerodendrum species such as *C. indicum, C. phlomidis, C. serratum var. amplexifolium, C. trichotomum, C. chinense, C. petasites* have been historically used as folk and traditional medicine to treat diseases, such as cold, hyperpyrexia, asthma, furunculosis, hypertension, rheumatism, dysentery, mammitis, toothache, anorexia, leucoderma, leprosy, arthrophlogosis, and other inflammatory diseases in numerous locations around the globe such as India, China, Korea, Japan, Thailand, and Africa[29–31]. The flowers of *C. paniculatum* have shown high antioxidant and hepatoprotective capacity while the flowers of *C. volubile* has shown effects on phagocytic respiratory burst indicating an immunomodulatory potential[32,33]. The stem, leaves and flowers contains triterpenes, steroids and flavonoids, and tribes use various parts of the plant in colic, scorpion sting and snake bite, smallpox, tumors and certain skin diseases[34–37]. Previous studies indicate the presence of the above secondary metabolites in plants, acting as key factors in the morphology and stabilization of nanoparticles. It makes the synthesis of AgNPs environmentally sustainable, inexpensive, and non-hazardous[38]. The current work intends to explore the in vitro anthelmintic activity of AgNPs generated from the aqueous floral extract of CLE on the cestode *Raillietina* spp. The study will evaluate the efficacy of the AgNPs as a potential anthelmintic treatment and contribute to understanding the mechanisms underlying their anthelmintic activity. The results of this study may provide new insights into the development of sustainable and eco-friendly treatments for helminth infections and help to address the problem of drug resistance in current treatments.

## Results

**Qualitative assessment of phytochemicals.** The therapeutic properties of the CLE flower can be associated with the presence of secondary metabolites such as alkaloids, flavonoids, saponins, phenols and tannins. Table 1 shows the phytochemical analysis of the aqueous extract from the flowers. These phytochemicals are vital in the reduction, capping, and stability of generated AgNPs, which also aid in averting nanoparticle agglomeration and enhancing their biological activity.

**UV–visible (UV–Vis) spectrophotometric analysis.** AgNPs exhibit a strong absorption band and generate specific color in solution due to the surface plasmon resonance (SPR)[39]. The colorless $AgNO_3$ solution became pale yellow after two hours and turned dark brown after 12 h of incubation at room temperature (Fig. 1a). The dark brown color observed at the end of the synthesis might occur at the 400–500 nm wavelength range due to the stimulation of surface plasmon vibrations specific to AgNPs[40]. The reduction of $Ag^+$ ion to $Ag^\circ$ during the reaction with the ingredients in CLE extract was observed by UV–Vis spectroscopy for the 350–1100 nm wavelength range. The magnitude of the absorption peak increased with reaction time due to the increased number of AgNPs. The maximum absorption of the CLE-AgNP sample was found at 405 nm (Fig. 1a), which confirmed the formation of the desired AgNPs.

**Fourier transform infrared spectroscopy (FTIR) analysis.** FTIR spectra were recorded to identify probable functional groups of the biomolecules present in CLE flower aqueous extract responsible for forming and stabilizing CLE-AgNPs (Fig. 1b and c). The strong bands in Fig. 1b at 3418, 2922, 2361, 1647, 1541, 1383, 1261, 1028, 808, and 669 $cm^{-1}$ corroborate with the capping agents responsible for the AgNPs formation. The vibration band at 3418 $cm^{-1}$ in the spectra is assigned to O–H stretching in alcohols and phenols. The peaks near 2912 and 2361 $cm^{-1}$ correspond to C–H and C–O or N–H stretching vibrations, respectively. The strong peak at

| Phytochemical constituents | Tests | Aqueous extract |
|---|---|---|
| Alkaloids | Mayer's test | + |
| Glycosides | Keller-Killiani test, Legal's test | – |
| Flavonoids | Alkaline reagent test | + |
| Tannins | Ferric chloride test | + |
| Saponins | Frothing test | + |
| Terpenoids | Concentrated $H_2SO_4$ test | + |
| Phenols | Ferric chloride test | + |

**Table 1.** Preliminary qualitative screening of the phytochemicals in the aqueous extract of CLE flower.

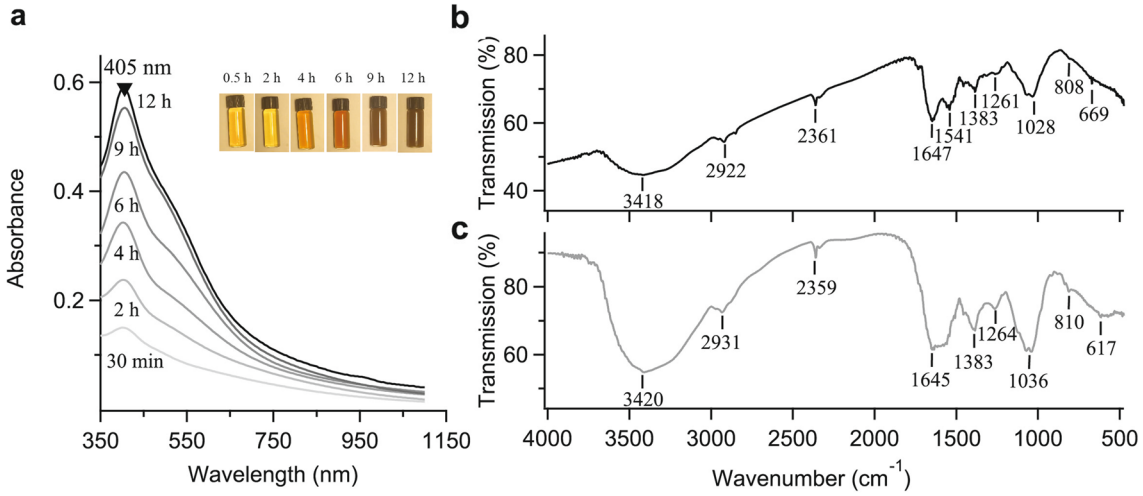


**Figure 1.** (**a**) UV-Visible spectra of AgNPs synthesized from CLE flower extract as a function of reaction time. (**b**) FTIR spectrum of aqueous extract of CLE. (**c**) FTIR spectrum of synthesized CLE-AgNPs.

1647 $cm^{-1}$ denotes C = O stretching arising due to the presence of the carbonyl group, indicating the presence of flavonoids and terpenoids. The peak at 1383 $cm^{-1}$ corresponds to C = O stretching vibration in carboxylic acids. The peak near 1261 $cm^{-1}$ corresponds to C–O stretching. The peaks near 1028 and 808 $cm^{-1}$ are assigned to amine C–N and C–H stretching, respectively. The spectra also showed a sharp peak at 669 $cm^{-1}$, corresponding to the N–H stretching of the primary and secondary amines and amides. FTIR analysis of CLE-AgNPs extract revealed similar absorption peaks around 3420, 2931, 2359, 1645, 1383, 1264, 1036, 810 and 617 $cm^{-1}$, indicating the presence of functional groups identical to AgNPs. A disappearance of peak at 1541 $cm^{-1}$ associated with polyols was noticed in the CLE-AgNP spectrum. The changes observed in FTIR spectra (Fig. 1b and c) conclude the association of phenols, flavonoids and terpenoids having functional groups of amide, amine, alcohol, carboxylic acids and ketones in the bioreduction reaction[9,41].

**X-ray diffraction (XRD) analysis.** To identify the crystalline phase and further confirm the AgNPs formation, the X-ray diffraction pattern of silver nanoparticles was recorded at UGC-DAE Consortium for Scientific Research, Kolkata (Bruker d8 Advance X-ray diffractometer, CuKα radiation (λ = 1.5406 Å), 40 kV– 40 mA, 2θ/θ scanning mode). Data was collected for the 2θ range of 20 to 80 degrees with a step of 0.0202 degree. The XRD patterns display four characteristic peaks at 38.188, 44.364, 64.53, and 77.485 Å (Fig. 2a). These peaks correspond to the crystal planes (111), (200), (220), and (311), respectively and match with the powdered diffraction standard values of Miller indices (*hkl*) of silver[40]. The diffraction angles corresponded to the face-centered cubic (FCC) structure of silver in AgNPs and agreed with the standard powder diffraction card of the Joint Committee on Powder Diffraction Standards (JCPDS) corresponding to silver (File No.: 04–0783)[42]. The average crystal size *D* of the AgNPs has been estimated from the diffractogram by using the Debye–Scherrer formula, $D = 0.9\lambda/\beta \mathrm{Cos}\theta$, where $\lambda$ is the wavelength of the X-rays used for diffraction, θ the Bragg angle, and $\beta$ the full width at half maximum (FWHM) of a diffraction band[43]. Based on the XRD spectrum of the CLE-AgNP, the average crystal size of the nanoparticles was calculated to be 27.67 nm.

**Scanning electron microscopy (SEM) studies.** The morphology of CLE-AgNPs characterized using SEM, revealed granular and spherical-shaped particles with diameters less than 50 nm, as shown in Fig. 2b. Some particles in the SEM image appear bigger than the average size due to nanoparticle aggregation caused by solvent evaporation due to critical point drying during the sample preparation.

**Transmission electron microscopy (TEM) studies.** The dispersion, aggregation, crystalline state and size of the CLE-AgNPs were examined using TEM, as shown in Fig. 2c. The sizes of CLE-AgNP particles were measured using ImageJ (https://imagej.nih.gov/ij/), and a histogram of sizes was calculated. The Gaussian fitting of the histogram yielded the mean particle size of CLE-AgNPs to be 27.75 ± 3.13 nm (mean ± sd, N = 90) (Fig. 2d). The surface morphology studied by TEM showed clear evidence for the metallic crystal formation of CLE-AgNPs, which was dispersed uniformly with fewer particle aggregation, and the particles formed in a spherical shape. The presence of some larger nanoparticles may be attributed to the fact that CLE-AgNPs tend to aggregate due to their high surface energy and high surface tension of the ultrafine nanoparticles[44].

**Efficacy of CLE-AgNP on *Raillietina* spp.** *Raillietina* spp., incubated in the control medium (PBS only), showed physical activity for a longer period; the controls survived for about 72.00 ± 0.04 h, following which they became immobilized and dead (Fig. 3). On exposure to the test medium CLE-AgNP and Genistein (reference drug), the parasites proceeded from the vigorous movement state to the relaxed state, following which they attained paralysis leading to death. The in vitro evaluation of the efficacy of CLE-AgNPs against the cestode

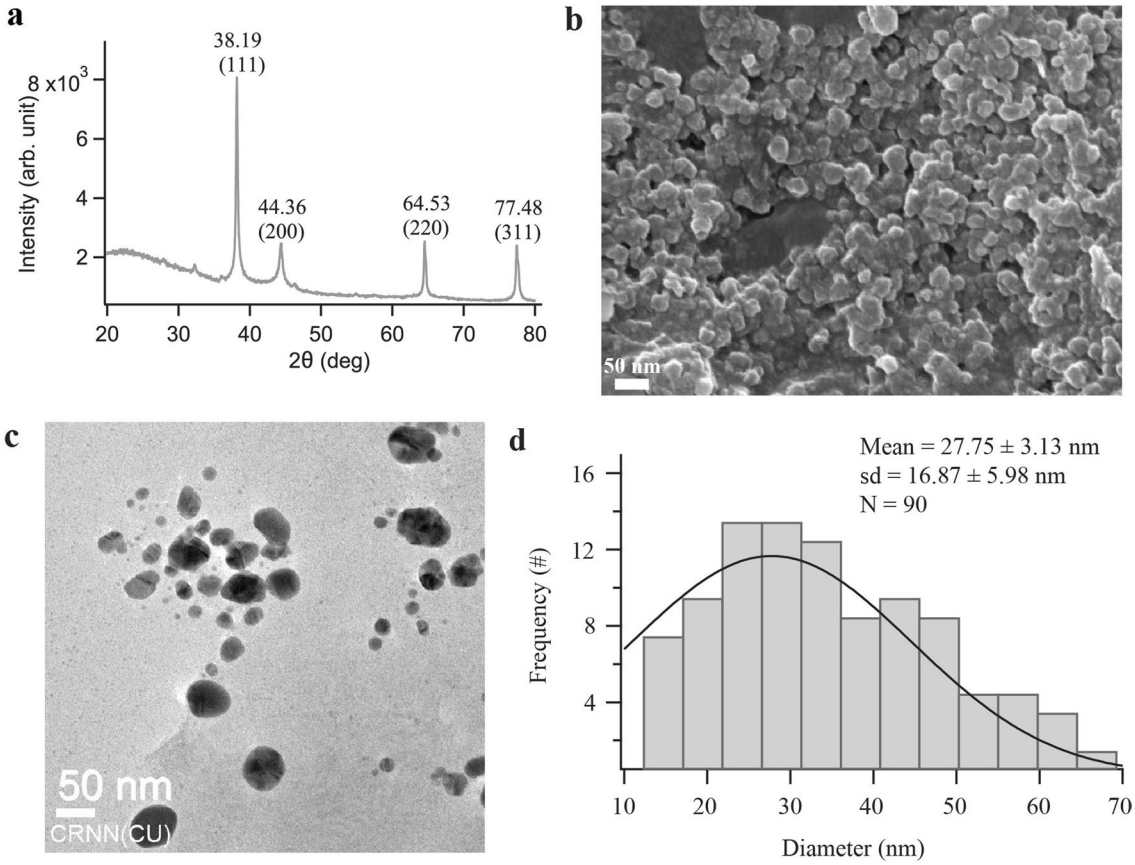


**Figure 2.** (**a**) X-ray diffraction patterns of synthesized CLE-AgNPs. (**b**) SEM micrograph of CLE-AgNPs (15 kV, 30 kX). (**c**) A typical TEM micrographic image of synthesized CLE-AgNPs. (**d**) CLE-AgNPs size distribution extracted from TEM images. The solid black curve is a Gaussian fit to the data.

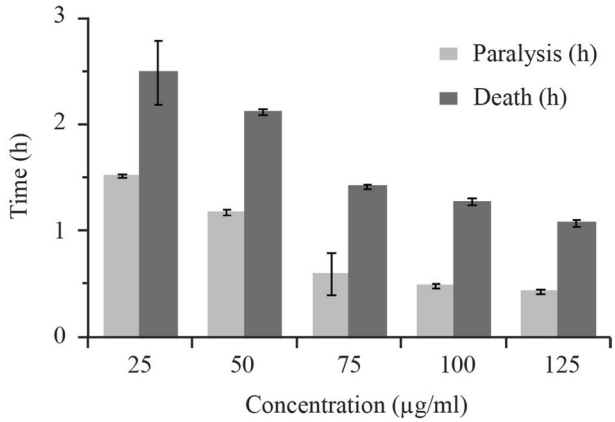


**Figure 3.** Results of CLE-AgNP efficacy on *Raillietina* spp. after exposure to five different concentrations (25, 50, 75, 100 and 125 µg/ml in PBS).

parasite showed a paralysis time within 1.51 h, 1.17 h, 0.59 h, 0.48 h, 0.43 h and death time of 2.48 h, 2.11 h, 1.41 h, 1.27 h, 1.07 h for dosages of 25, 50, 75, 100, and 125 µg/ml, respectively. We observed reduced anthelmintic effects on the cestode parasite when exposed to CLE-aqueous extract only (Supplementary Table S1).

**Morphological changes of CLE-AgNP-exposed *Raillietina* spp.** SEM images of the control parasites reveal a rostellum and four suckers arranged sideways around the scolex, each with circlets of broad hooks at the bottom, tapered, and bent toward the ends (Fig. 4a). At higher magnification, the surface tegument of the proglottid is revealed to be covered with smooth, homogenous microtriches, which are the absorptive structures

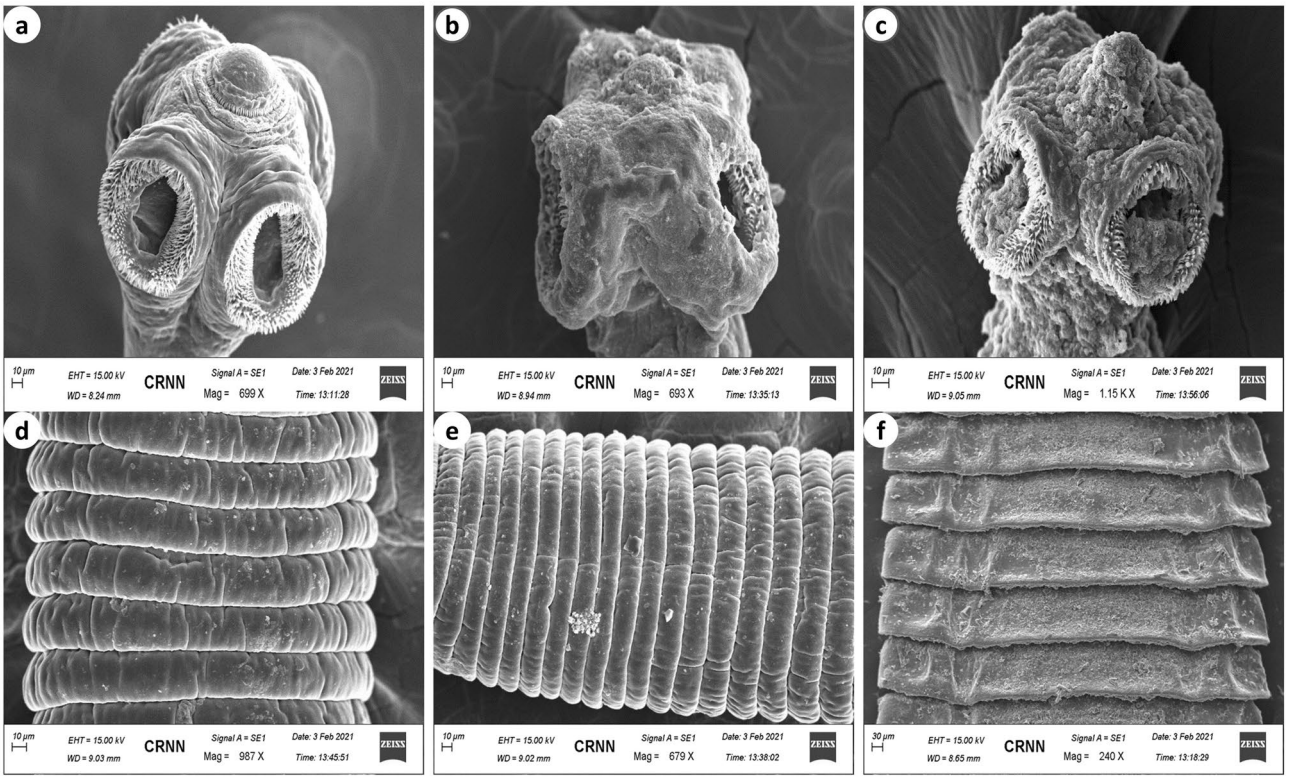


**Figure 4.** Scanning electron micrographs of control worm ((**a**) scolex, (**d**) gravid proglottid), Genistein ((**b**) scolex, (**e**) gravid proglottid) and silver nanoparticle exposed *Raillietina* spp. ((**c**) scolex, (**f**) gravid proglottid).

for feeding (Fig. 4d). However, on exposure to the test medium, the general surface topography of the proglottids degenerated with the formation of wrinkles (Fig. 4f). The cestode treated with CLE-AgNP showed irrevocable destruction of the scolex, which appeared greatly distorted with suckers extensively shrunken and sharply crooked spines around the suckers. The filamentous nature of microtriches was lost, and the spines around suckers were broken and eroded (Fig. 4c), which altered the maintenance of the parasite position on the host cell, affecting its nutrition. The Genistein-treated parasites showed immense disfigurement of the scolex, breakage and disembarkment of the tegumental surface structures (Figs. 4b, e).

**Histochemical studies.** The tegument (T) of the control *Raillietina* spp. showed intense activity of Acid phosphatase (AcPase), Acid phosphatase (AlkPase), Adenosine triphosphatase (ATPase) and 5'-Nucleotidase (5'-Nu) compared to sub-tegument (ST) and somatic musculature (SM) (Fig. 5a–d). Figure 5e–h depict the histological sections of CLE-AgNP exposed parasites showing a general reduction in the staining intensity in the T, ST and SM, whereas the parenchyma cells (P) remained unaffected. AcPase showed a pronounced reduction in stain intensity in the T and ST region for the AgNP incubated section (Fig. 5a,e), indicating disruption of the parasitic membrane transport metabolism. However, there was minimal activity throughout the section of parasites exposed to Genistein (Fig. 5i–l). A much-diminished activity of AlkPase was observed throughout the treated sections of the parasite (Fig. 5b,f). The ATPase activity was almost imperceptible in the T and ST of the parasite treated with CLE-AgNP compared to the control parasites (Fig. 5c,g). The 5'-Nu activity was also found to be reduced throughout the T and ST region in the AgNP exposed cestodes compared to the control (Fig. 5d,h). The decrease in the enzymatic activities resulted from the tegumental damages caused by the CLE-AgNPs.

## Discussion

We utilized Clerodendrum flowers for the extracellular production of silver nanoparticles and demonstrated their capabilities as an alternative to synthetic chemical techniques. In recent times, the synthesis of nanoparticles from natural sources has gained immense publicity. Organic nanoparticles such as chitosan and lipid nanoparticles and inorganic nanoparticles such as gold have been used as nano-drug delivery systems[45–49]. The mode of bactericidal effect of nanoparticles has not yet been fully elucidated. However, it irreversibly disrupts the bacterial cell wall, inactivates vital proteins, chelates DNA, and forms reactive oxygen species known to have high microbicidal activity[41,49–52]. While microorganisms continue to be investigated for metal nanoparticle synthesis, using plant extracts in the biosynthesis of nanoparticle manufacturing processes is an attractive prospect that is yet largely unknown and underutilized. In the current investigation, we focused on the green synthesis of CLE-AgNP by adding plant extract to the $AgNO_3$ solution (Fig. 6a), which was initially confirmed by the color changes of the solution from colorless to pale yellow and later measured spectrophotometrically (Fig. 1a). The intensity of

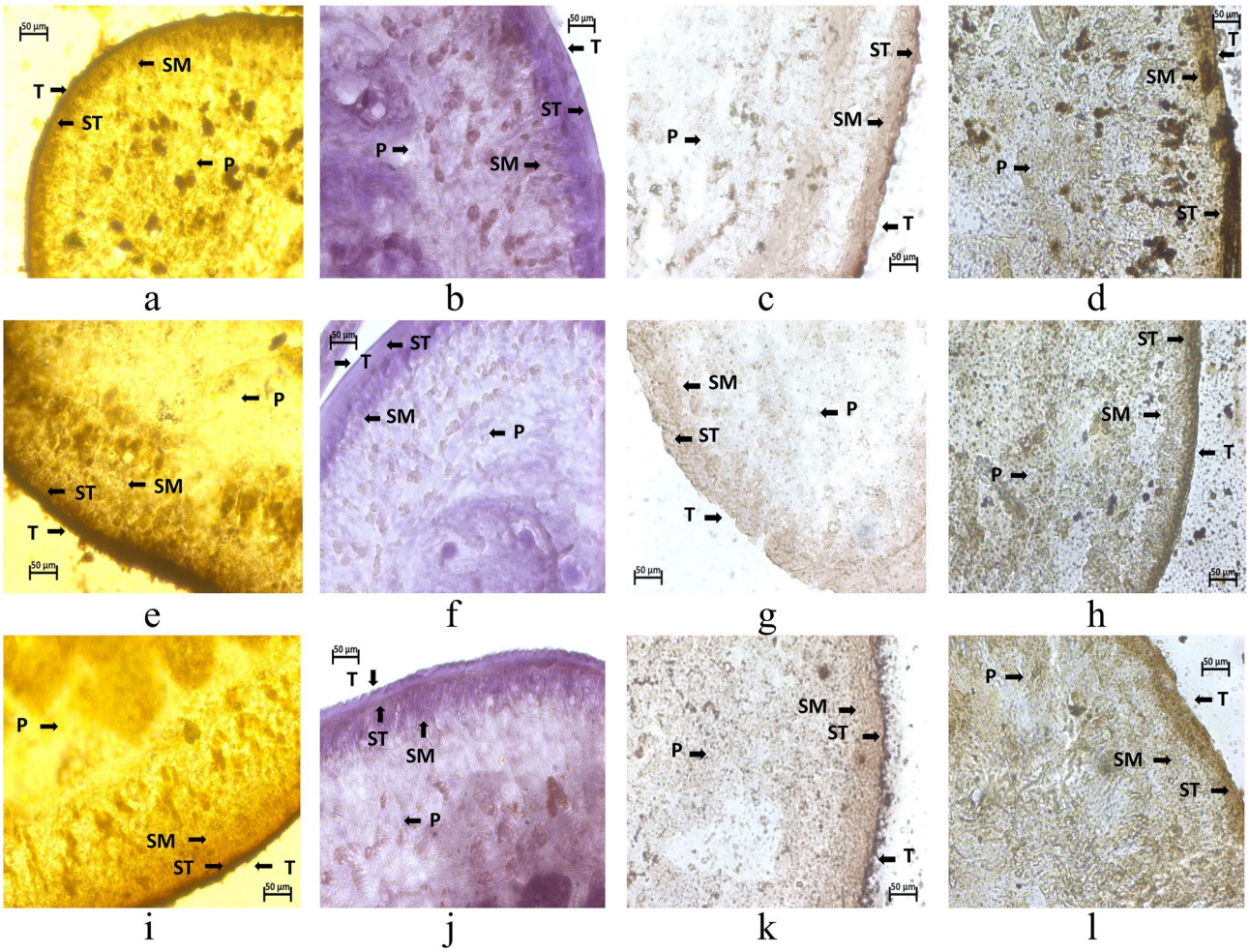


**Figure 5.** Histochemical demonstration of AcPase (**a**,**e**,**i**), AlkPase (**b**,**f**,**j**), ATPase (**c**,**g**,**k**) and 5'-Nu (**d**,**h**,**l**) activities in *Raillietina* spp. treated with (125 µg/ml) and Genistein (125 µg/ml); (**a–d**) Transverse section of control parasite; (**e–h**) AgNPs -exposed parasite; (**i–l**): Genistein-exposed parasite. All scale bars correspond to 50 µm.

the color increased in direct proportion to the incubation period, and the highest absorption peak indicated the maximal yield. Previous research has indicated that plants contain phenols and flavonoids with great antioxidant functions, enabling the synthesis of nanoparticles[53,54]. Evidence identifying various phytoconstituents in *C. infortunatum* flower screened for flavonoids, saponins, phenol, and tannins with potential therapeutic pursuits rationalized our objective for preparing CLE-AgNPs. Although the exact underlying mechanism for forming AgNPs is unclear, it has been proposed that the various active functional groups of phytochemicals in CLE flower are responsible for biosynthesis AgNPs by reducing Ag ions to their elemental form[55,56] (Fig. 6b). Bioreduction of silver ions is followed by nucleation and growth of the adjacent reduced silver atoms into silver nanoparticles of characteristic shape and size. Finally, the newly synthesized nanoparticles are stabilized by capping with the phytochemicals. The capping agents were confirmed by the FTIR analyses of the nanoparticles. For CLE-AgNPs, we observed that most of the functional groups present in the flower aqueous extract were intact in the synthesized nanoparticle. The absorption bands mainly represented the presence of functional groups such as phenol, ketones, carboxylic acids, amines and amides. Compared to the CLE flower extract, the FTIR measurements of CLE-AgNP showed the disappearance of peak at 1541 $cm^{-1}$, indicating that the polyols like flavonoids and terpenoids in CLE extract are primarily responsible for reducing silver ions. The shift of peak from 669 $cm^{-1}$ to 617 $cm^{-1}$ in the absorption peaks suggests that the amine components are involved in reducing and stabilizing the nanoparticles. (Fig. 1b,c). Further, the sharp peak at 1645 $cm^{-1}$ indicated the presence of flavonoids and terpenoids that complied with the reports of the qualitative study of phytochemicals (Table 1). In a similar study, Jayakumar et al. demonstrated the use of FTIR to detect biomolecules for reducing $Ag^{+}$ ions and capping *Clerodendrum splendens* extract-produced AgNPs[57]. CLE-AgNP was crystalline, mostly spherical, with variable particle size and elemental (Fig. 2a) in nature. The crystallite size of the material from XRD measurements was found to be around 27.67 nm. In addition to the four major XRD peaks in the diffractogram, other unidentified peaks observed might be attributed to the formation of the crystalline biomolecules bound to the surface of the AgNPs. SEM and TEM analysis also confirmed the synthesis of variable size (12–44 nm, mean ≈ 27) and spherical shape AgNPs (Fig. 2b–d).

Recent studies indicate that smaller nanoparticles are useful for delivering many targets, especially antimicrobial activity, as they have more surface exposure to the bacterial membrane increasing the cell permeability and resulting in cell death[58]. Their small sizes also allow efficient drug accumulation at the target sites with provisions for sustained drug release[59]. The results shown in Fig. 4 demonstrate that CLE-AgNP indeed has anthelmintic efficacy on poultry cestode *Raillietina* spp. and acts in a dose and time-dependent manner. The individual impact of CLE flower extract at the highest dose (125 µg/ml) was 2.75 ± 0.1 h and 3.21 ± 0.14 h for paralysis and death, respectively, while its anthelmintic activity was enhanced when combined with silver particles (Supplementary Table S1). Previous studies suggest phytochemicals and their stabilization properties may have a profound colloidal activity causing a synergistic impact on one another when the extract is coated on AgNPs[60]. The most efficacious dose of CLE-AgNP was 125 µg/ml, wherein the initiation of paralysis of parasites occurred after 0.43 h and death after 1.07 h of treatment (Fig. 4). Scanning electron microscopy results have shown discernible topographical mutilation on test worms, while control tapeworm shows smooth and organized rostellum, sucker, and microtriches on the head and strobila portion. As observed in the present investigation, tegumental erosion has altered the host-parasite interface, causing severe nutrient deficiency within the parasite. Apart from the absorption of nutrients, the possible role of spine-like features of the microtriches is holding with its host to maintain its position in the gut. Therefore, disruption of microtriches leads to reduced attachment capacity of the parasites to the host. Similar observations were recorded on incubation of the parasite in Resveratrol, which causes blebbing, swelling of the tegument, loss of spines and distortion of suckers in *Raillietina* spp. exposed in vitro[61]. Extensive blebbing of *Fasciola hepatica* surface was seen on treatment with various concentrations of crude ethanolic shoot extract of traditionally used medicinal plants like *Alpinia nigra*[62]. Other phytocompounds like α-viniferin have been unequivocally responsible for damages in varying degrees on the teguments of cestodes[63]. In a recent study, the tegument and suckers of the tapeworm *Raillietina tetragona* and the cuticle and lips of the roundworm *Ascardia galli* both showed rigorous damage on treatment with the roots and rhizomes extract of an ethnomedicinal plant *Imperata cylindrica*[64]. The tegumental enzymes AcPase and AlkPase are found to be involved in the uptake of certain nutrients, glycogen and lipoprotein in various helminth parasites[65]. Enzymatic alterations in histochemical localization studies also revealed pronounced effects (Table 2). ATPase is associated with active

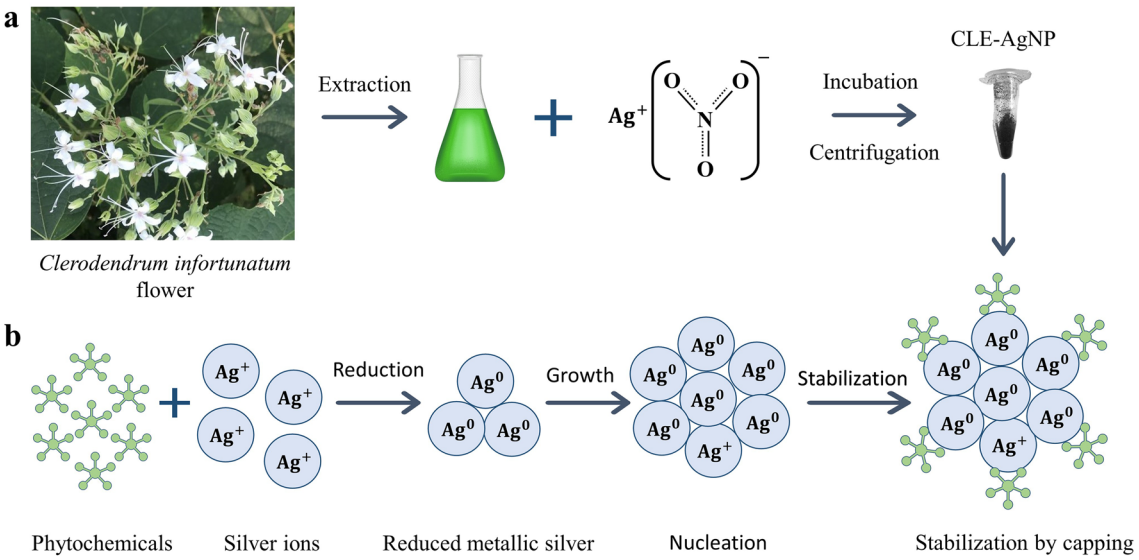


**Figure 6.** A schematic figure depicting the (**a**) plant mediated synthesis of silver nanoparticles (**b**) possible underlying mechanism of CLE-AgNP synthesis from the plant metabolites.

| Treatment | Distribution of enzyme activity | | | | | | | | | | | | | | | |
|---|---|---|---|---|---|---|---|---|---|---|---|---|---|---|---|---|
| | AcPase | | | | AlkPase | | | | ATPase | | | | 5'-Nu | | | |
| | T | ST | SM | P | T | ST | SM | P | T | ST | SM | P | T | ST | SM | P |
| Control (0.9% PBS) | ++++ | +++ | +++ | ++ | +++ | + | ++ | +/− | ++++ | ++ | +++ | +/+ | ++++ | +++ | ++ | +/+ |
| Genistein (125 µg/ml) | − | − | + | − | − | ++ | ++ | − | + | − | + | +/+ | + | + | ++ | −/− |
| AgNP (125 µg/ml) | − | − | + | − | + | − | − | − | + | − | − | − | − | − | − | − |

**Table 2.** Summary of histochemical localization activities of AcPase, AlkPase, ATPase and 5'-Nu in the various structures of *Raillietina* spp. ++++ = very intense activity, +++ = intense activity, + = mild activity, − = no activity.

transport, and a significant reduction in its activity in the somatic musculature, and complete absence in the tegument and sub-tegumental layers in 125 µg/ml CLE-AgNP-exposed parasite further indicates the disruption of the energy metabolism pathway in the parasite. In a previous study, following treatment with Genistein, the active component of *Flemingia vestita*, the tegumental enzymes like AcPase, AlkPase, ATPase and 5'-Nu of *Raillietina* spp. were found to be decreased many folds[66]. Thus, the observed decrease in the two tegumental phosphatase activities might be related to inhibition or decreased glucose absorption by *Raillietina* spp., resulting in progressive loss of motor function owing to a deficiency of energy source and, eventually, paralysis and death.

In summary, our investigation elucidates a concise, cost-effective, and productive route in the phytosynthesis of AgNPs utilizing the aqueous floral extract of CLE. Further, in vivo, studies are required to understand the mode of action of the drug and its pharmacokinetics. In the future, optimization of the test therapeutic (CLE-AgNP) through pharmaceutical evaluation and application of appropriate feeding strategy by finding out the effects on metabolic precursors and intracellular metabolites can contribute to a seamless transition to financially feasible ethnomedicinal anthelmintic. We believe using green synthesis methods to produce silver nanoparticles from *Clerodendrum infortunatum* flowers could provide a promising alternative to synthetic anthelmintic drugs for treating helminth infections in domestic fowl.

## Materials and methods

**Collection of plant material.** The fresh and healthy flowers of *Clerodendrum infortunatum* were collected from the Cooch Behar Panchanan Barma University (CBPBU) campus garden (latitude 26.321796 °N, longitude 89.469329 °E) over a time of 2 months between May to June 2021. Dr. Chaya Deori did the taxonomical evaluation, and the voucher specimen (AC-97296) was kept at the herbarium of the Botanical Survey of India, Eastern Regional Centre, Shillong. We confirm that the collection of plant material complied with relevant institutional, national, and international guidelines and legislation. The appropriate permissions for collecting plant specimens were obtained from the CBPBU administration affiliated with the Government of West Bengal, India.

**Preparation of plant extract using flowers of CLE.** The flowers were thoroughly washed sequentially with tap and deionized water, air-dried and chopped into small pieces. Chopped flowers (20 g) were added to 100 ml deionized autoclaved water in a beaker and heated at 90 °C in a temperature-controlled water bath for 10 min. The extract was cooled, filtered through Whatman No. 1 filter paper, and kept at 4 °C until used.

**Qualitative assessment of phytochemicals.** The phytochemical analysis of *Clerodendrum infortunatum* flower extract was carried out using aqueous extracts using standard procedures outlined in Table 1, with minor modifications to identify the various constituents.

**Biosynthesis of CLE-capped AgNP.** For silver nanoparticle synthesis, about 10 mL of CLE flower extract was added to a 90 mL aqueous solution of 1 mM $AgNO_3$ (Merck Laboratories, India) and kept at room temperature. The color changed from pale yellow to brown, indicating the formation of the AgNPs due to the reaction of flower extracts of CLE with silver metal ions. Control was maintained without adding flower extract in the silver nitrate solution that showed no color changes. The purified AgNPs were obtained by removing the extract by centrifuging the suspension thrice at 15,000 rpm for 20 min, followed by washing it twice with double sterilized water.

**Characterization studies of AgNP.** Visible colour changes preliminarily determined the bio-reduction process of silver ions in solution and later monitored using UV–visible absorption spectroscopy (Hitachi U-2900). The synthesized AgNPs were freeze-dried, powdered, and used for XRD analysis. The dried powder was mixed with potassium bromide at the ratio of 1:100, and the results were recorded using FTIR (Jasco FR/IR-6300). The CLE-AgNPs were critical point dried, placed over a carbon tape onto an SEM stub, platinum coated, and viewed under a scanning electron microscope (Zeiss EVO-18) at a voltage of 15 kV to assess the surface morphology of the biogenic AgNPs. Transmission electron microscopy (JEOL JEM-2100 HR) was used to understand the size and morphology of AgNPs.

**Collection of parasites and in vitro treatment.** Live mature *Raillietina* spp. (Megnin, 1880) (Class: Cestoda; Order: Cyclophyllidea; Family: Davaineidae) were collected from the intestine of freshly sacrificed domestic fowl (*Gallus gallus domesticus* L.) from local abattoirs in Cooch Behar and maintained in 0.9% PBS at 37 ± 1°C in an incubator. Control parasites were maintained in 0.9% PBS (pH 7.2) at 37 ± 1°C, whereas for treatment, live worms were directly incubated in different concentrations of test treatment (25, 50, 75, 100, 125 µg/ml) in separate Petri dishes, both for the CLE flower aqueous extract and CLE-AgNPs. Similarly, treatment was also performed with Genistein at a dose of 125 µg/ml of PBS as a broad-spectrum reference drug. Six replicates for each set of incubation mediums were prepared, and the time taken to attain the paralytic state and death was recorded. Mortality of parasites was confirmed by removing treated parasites from the test medium and dipping them in slightly lukewarm water, which was indicated by the cessation of all signs of movement. The control and CLE-AgNP treated parasites were retrieved from the respective incubation mediums and processed for histochemical and electron microscopic studies.

**Scanning electron microscopy of the parasite.** The parasites were fixed in 10% neutral buffered formalin for 24 h immediately after paralysis. After fixation, the sample was rinsed in PBS and dehydrated with acetone grades ranging from pure dry acetone to escalating degrees of acetone. The specimens were then critical-

point dried using liquid carbon dioxide as the transitional fluid, which was put on a metal stub and coated with platinum in a fine-coat ion sputter, JFC-1100 (JEOL). The specimens were then viewed using a Zeiss EVO-18 (Special edition) scanning electron microscope at an accelerating voltage of 10–15 kV.

**Histochemical studies.** The tegumental enzymes were investigated histochemically using duly processed frozen sections cut at a thickness of 10–12 µm in a Leica CM 3050S cryostat. AcPase activity was detected in cold formol calcium fixed specimens following the modified lead nitrate method[67], using sodium β-phosphoglycerate as the substrate, where a brownish precipitate on tegumental sections indicates the sites of AcPase activity. The modified coupling azo-dye method assessed AlkPase activity at room temperature (17–20 °C). The calcium method of Pearse was implemented to detect the localization of ATPase activity, where adenosine triphosphate was used as the substrate, and the enzyme activity was determined by observing blackish-brown deposits[67]. To observe 5'-Nu, the lead method of Wachstein and Meisel was employed using adenosine monophosphate as a substrate[68]. The histological sections were viewed using Carl Zeiss Axiolab 5 Phase Contrast Microscope.

**Ethics approval.** We confirm that any aspect of the work covered in this manuscript does not involve ethical approval.

## Data availability

The data used to substantiate the findings of this study are included in the article; however, the raw data is also available from the corresponding author upon request.

Received: 14 March 2023; Accepted: 26 April 2023
Published online: 07 May 2023

## References

1. Permin, A. & Hansen, J. W. *Epidemiology, Diagnosis and Control of Poultry Parasites* (Fao, 1998).
2. Samad, M. A., Alam, M. M. & Bari, A. S. M. Effect of *Raillietina echinobothrida* infection on blood values and intestinal tissues of domestic fowls of Bangladesh. *Vet. Parasitol.* **21**, 279–284 (1986).
3. Zirintunda, G. *et al.* Emerging anthelmintic resistance in poultry: Can ethnopharmacological approaches offer a solution?. *Front. Pharmacol.* **12**, 3722 (2022).
4. Pagar, T., Ghotekar, S., Pagar, K., Pansambal, S. & Oza, R. A review on bio-synthesized $Co_3O_4$ nanoparticles using plant extracts and their diverse applications. *J. Chem. Rev.* **1**, 260–270 (2019).
5. Zikalala, N., Matshetshe, K., Parani, S. & Oluwafemi, O. S. Biosynthesis protocols for colloidal metal oxide nanoparticles. *Nano-Struct. Nano-Objects* **16**, 288–299 (2018).
6. Lu, H. *et al.* Bioengineered microbial platforms for biomass-derived biofuel production–A review. *Chemosphere* **288**, 132528 (2022).
7. Changmai, B., Vanlalveni, C., Ingle, A. P., Bhagat, R. & Rokhum, S. L. Widely used catalysts in biodiesel production: A review. *RSC Adv.* **10**, 41625–41679 (2020).
8. Simon, S. *et al.* Biomedical applications of plant extract-synthesized silver nanoparticles. *Biomedicines* **10**, 2792 (2022).
9. Al-Otibi, F. *et al.* Biosynthesis of silver nanoparticles using *Malva parviflora* and their antifungal activity. *Saudi J. Biol. Sci.* **28**, 2229–2235 (2021).
10. Dappula, S. S. *et al.* Biosynthesis of zinc oxide nanoparticles using aqueous extract of *Andrographis alata*: Characterization, optimization and assessment of their antibacterial, antioxidant, antidiabetic and anti-Alzheimer's properties. *J. Mol. Struct.* **1273**, 134264 (2023).
11. Kang, J. P. *et al.* Biosynthesis of gold and silver chloride nanoparticles mediated by *Crataegus pinnatifida* fruit extract: In vitro study of anti-inflammatory activities. *Artif. Cells Nanomed. Biotechnol.* **46**, 1530–1540 (2018).
12. Sargazi, S. *et al.* Application of green gold nanoparticles in cancer therapy and diagnosis. *Nanomaterials* **12**, 1102 (2022).
13. Prathna, T., Chandrasekaran, N., Raichur, A. M. & Mukherjee, A. Biomimetic synthesis of silver nanoparticles by *Citrus limon* (lemon) aqueous extract and theoretical prediction of particle size. *Colloids Surf. B Biointerfaces* **82**, 152–159 (2011).
14. Kaur, M., Gautam, A., Guleria, P., Singh, K. & Kumar, V. Green synthesis of metal nanoparticles and their environmental applications. *Curr. Opin. Environ. Sci. Health* **29**, 100390 (2022).
15. Hasan, K. F. *et al.* Functional silver nanoparticles synthesis from sustainable point of view: 2000 to 2023-A review on game changing materials. *Heliyon* **8**, e12322 (2022).
16. Mittal, J., Batra, A., Singh, A. & Sharma, M. M. Phytofabrication of nanoparticles through plant as nanofactories. *Adv. Nat. Sci.* **5**, 043002 (2014).
17. Mickymaray, S. One-step synthesis of silver nanoparticles using Saudi Arabian desert seasonal plant *Sisymbrium irio* and antibacterial activity against multidrug-resistant bacterial strains. *Biomolecules* **9**, 662 (2019).
18. Mohanta, Y. K. *et al.* Phyto-assisted synthesis of bio-functionalised silver nanoparticles and their potential anti-oxidant, antimicrobial and wound healing activities. *IET Nanobiotechnol.* **11**, 1027–1034 (2017).
19. Jha, A. K., Prasad, K., Prasad, K. & Kulkarni, A. Plant system: Nature's nanofactory. *Colloids Surf. B Biointerfaces* **73**, 219–223 (2009).
20. Annamalai, N., Thavasi, R., Vijayalakshmi, S. & Balasubramanian, T. A novel thermostable and halostable carboxymethylcellulase from marine bacterium *Bacillus licheniformis* AU01. *World J. Microbiol. Biotechnol.* **27**, 2111–2115 (2011).
21. Alhujaily, M. *et al.* Recent advances in plant-mediated zinc oxide nanoparticles with their significant biomedical properties. *Bioengineering* **9**, 541 (2022).
22. Adeyemi, J. O., Onwudiwe, D. C. & Oyedeji, A. O. Biogenic synthesis of CuO, ZnO, and CuO–ZnO nanoparticles using leaf extracts of *Dovyalis caffra* and their biological properties. *Molecules* **27**, 3206 (2022).
23. Kurian, J. T., Chandran, P. & Sebastian, J. K. Synthesis of inorganic nanoparticles using traditionally used Indian medicinal plants. *J. Clust. Sci.* https://doi.org/10.1007/s10876-022-02403-6 (2022).
24. Thrilokaraj, T. R. *et al.* A Sustainable Approach for Nickel Nanoparticles Synthesis: An Expeditious Access to N-heterocycles under Heterogeneous Condition and its Photophysical studies. *New J. Chem.* **47**, 8268–8276 (2023).
25. Rai, M. & Yadav, A. Plants as potential synthesizer of precious metal nanoparticles: Progress and prospects. *IET Nanobiotechnol.* **7**, 117–124 (2013).
26. Tripathi, R., Saxena, A., Gupta, N., Kapoor, H. & Singh, R. High antibacterial activity of silver nanoballs against *E. coli* MTCC 1302, *S. typhimurium* MTCC 1254, *B. subtilis* MTCC 1133 and *P. aeruginosa* MTCC 2295. *Dig. J. Nanomater. Bios.* **5**, 323–330 (2010).

27. Kar, P. K., Murmu, S., Saha, S., Tandon, V. & Acharya, K. Anthelmintic efficacy of gold nanoparticles derived from a phytopathogenic fungus, *Nigrospora oryzae*. *PLoS ONE* **9**, e84693 (2014).
28. Srivastava, M. & Shanker, K. *Duranta erecta* Linn: A critical review on phytochemistry, traditional uses, pharmacology, and toxicity from phytopharmaceutical perspective. *J. Ethnopharmacol.* **293**, 115274 (2022).
29. Shrivastava, N. & Patel, T. *Clerodendrum* and healthcare: An overview. *Med. Aromat. Plant Sci. Biotechnol.* **1**, 142–150 (2007).
30. Baker, J. T. *et al.* Natural product drug discovery and development: New perspectives on international collaboration. *J. Nat. Prod.* **58**, 1325–1357 (1995).
31. Hazekamp, A., Verpoorte, R. & Panthong, A. Isolation of a bronchodilator flavonoid from the Thai medicinal plant *Clerodendrum petasites*. *J. Ethnopharmacol.* **78**, 45–49 (2001).
32. Kopilakkal, R., Chanda, K. & Balamurali, M. M. Hepatoprotective and antioxidant capacity of *Clerodendrum paniculatum* flower extracts against carbon tetrachloride-induced hepatotoxicity in rats. *ACS Omega* **6**, 26489–26498 (2021).
33. Erukainure, O. L. *et al.* Flowers of *Clerodendrum volubile* exacerbate immunomodulation by suppressing phagocytic oxidative burst and modulation of COX-2 activity. *Biomed. Pharmacother.* **83**, 1478–1484 (2016).
34. Akihisa, T. *et al.* The 24α-and 24β-epimers of 24-ethylcholesta-5, 22-dien-3β-ol in two *Clerodendrum* species. *Phytochemistry* **27**, 1169–1172 (1988).
35. Sinha, N., Seth, K., Pandey, V., Dasgupta, B. & Shah, A. Flavonoids from the flowers of *Clerodendron infortunatum*. *Planta Med.* **42**, 296–298 (1981).
36. Manzoor-Khuda, M. & Sarela, S. Constituents of *Clerodendron infortunatum* (bhat)—I: Isolation of clerodolone, clerodone, clerodol and clerosterol. *Tetrahedron* **21**, 797–802 (1965).
37. Wang, J.-H., Luan, F., He, X.-D., Wang, Y. & Li, M.-X. Traditional uses and pharmacological properties of *Clerodendrum* phytochemicals. *J. Tradit. Complement. Med.* **8**, 24–38 (2018).
38. Mohanta, Y. K. *et al.* Antimicrobial, antioxidant and cytotoxic activity of silver nanoparticles synthesized by leaf extract of *Erythrina suberosa* (Roxb.). *Front. Mol. Biosci.* **4**, 14 (2017).
39. Mehata, M. S. Surface plasmon resonance allied applications of silver nanoflowers synthesized from *Breynia vitis-idaea* leaf extract. *Dalton Trans.* **51**, 2726–2736 (2022).
40. Krishnaraj, C. *et al.* Synthesis of silver nanoparticles using *Acalypha indica* leaf extracts and its antibacterial activity against water borne pathogens. *Colloids Surf. B Biointerfaces* **76**, 50–56 (2010).
41. Govarthanan, M. *et al.* Low-cost and eco-friendly synthesis of silver nanoparticles using coconut (*Cocos nucifera*) oil cake extract and its antibacterial activity. *Artif. Cells Nanomed. Biotechnol.* **44**, 1878–1882 (2016).
42. Gates-Rector, S. & Blanton, T. The powder diffraction file: A quality materials characterization database. *Powder Diffr.* **34**, 352–360 (2019).
43. Selvanayaki, R. *et al.* Structural, optical and electrical conductivity studies of pure and Fe doped ZincOxide (ZnO) nanoparticles. *Mater. Today* **49**, 2628–2631 (2022).
44. Theivasanthi, T. & Alagar, M. Electrolytic synthesis and characterizations of silver nanopowder. Preprint at https://arXiv.org/quant-ph/1111.0260 (2011).
45. Ssekatawa, K. *et al.* Prevalence of pathogenic *Klebsiella pneumoniae* based on PCR capsular typing harbouring carbapenemases encoding genes in Uganda tertiary hospitals. *Antimicrob. Resist. Infect. Control* **10**, 1–10 (2021).
46. Patra, J. K. *et al.* Nano based drug delivery systems: Recent developments and future prospects. *J. Nanobiotechnol.* **16**, 1–33 (2018).
47. Rai, S., Singh, N. & Bhattacharya, S. Concepts on smart nano-based drug delivery system. *Recent Pat. Nanotechnol.* **16**, 67–89 (2022).
48. Xiao, H. *et al.* Inorganic nanocarriers for platinum drug delivery. *Mater. Today* **18**, 554–564 (2015).
49. Kandiah, M. & Chandrasekaran, K. N. Green synthesis of silver nanoparticles using *Catharanthus roseus* flower extracts and the determination of their antioxidant, antimicrobial, and photocatalytic activity. *J. Nanotechnol.* **2021**, 5512786 (2021).
50. Rizzello, L., Cingolani, R. & Pompa, P. P. Nanotechnology tools for antibacterial materials. *Nanomedicine* **8**, 807–821 (2013).
51. Mythili, R. *et al.* Utilization of market vegetable waste for silver nanoparticle synthesis and its antibacterial activity. *Mater. Lett.* **225**, 101–104 (2018).
52. Ameen, F. *et al.* Phytosynthesis of silver nanoparticles using *Mangifera indica* flower extract as bioreductant and their broad-spectrum antibacterial activity. *Bioorg. Chem.* **88**, 102970 (2019).
53. Mohanta, Y. K. *et al.* Bio-inspired synthesis of silver nanoparticles from leaf extracts of Cleistanthus collinus (Roxb.): Its potential antibacterial and anticancer activities. *IET Nanobiotechnol.* **12**, 343–348 (2018).
54. Hegde, R. V. *et al.* Biogenic synthesis of Pd-nanoparticles using areca nut husk extract: A greener approach to access α-keto imides and stilbenes. *New J. Chem.* **45**, 16213–16222 (2021).
55. Mohanta, Y. K., Panda, S. K., Bastia, A. K. & Mohanta, T. K. Biosynthesis of silver nanoparticles from *Protium serratum* and investigation of their potential impacts on food safety and control. *Front. Microbiol.* **8**, 626 (2017).
56. Limaye, A. S. *et al.* Greener Approach for Pd–NPs Synthesis Using *Mangifera indica* Leaf Extract: Heterogeneous Nano Catalyst for Direct C–H Arylation of (Poly) Fluorobenzene, Hiyama Coupling Reaction and Hydrogen Evolution Reaction Study. *Catal. Lett.* 1–17. https://doi.org/10.1007/s10562-022-04138-5 (2022).
57. Jayakumar, A. & Vedhaiyan, R. K. Rapid synthesis of phytogenic silver nanoparticles using *Clerodendrum splendens*: Its antibacterial and antioxidant activities. *Korean J. Chem. Eng.* **36**, 1869–1881 (2019).
58. Azizian-Shermeh, O., Jalali-Nezhad, A. A., Taherizadeh, M. & Qasemi, A. Facile, low-cost and rapid phytosynthesis of stable and eco-friendly silver nanoparticles using *Boerhavia elegans* (Choisy) and study of their antimicrobial activities. *J. Inorg. Organomet. Polym. Mater.* **31**, 279–291 (2021).
59. Patil, M. P. & Kim, G.-D. Eco-friendly approach for nanoparticles synthesis and mechanism behind antibacterial activity of silver and anticancer activity of gold nanoparticles. *Appl. Microbiol. Biotechnol.* **101**, 79–92 (2017).
60. Bélteky, P. *et al.* Silver nanoparticles: Aggregation behavior in biorelevant conditions and its impact on biological activity. *Int. J. Nanomed.* **14**, 667 (2019).
61. Giri, B. R. & Roy, B. Resveratrol induced structural and biochemical alterations in the tegument of *Raillietina echinobothrida*. *Parasitol. Int.* **63**, 432–437 (2014).
62. Roy, B. & Swargiary, A. Anthelmintic efficacy of ethanolic shoot extract of *Alpinia nigra* on tegumental enzymes of *Fasciolopsis buski*, a giant intestinal parasite. *J. Parasit. Dis.* **33**, 48–53 (2009).
63. Roy, B. & Giri, B. R. α-Viniferin-induced structural and functional alterations in *Raillietina echinobothrida*, a poultry tapeworm. *Microsc. Microanal.* **21**, 377–384 (2015).
64. Lalthanpuii, P. B. & Lalchhandama, K. Phytochemical analysis and in vitro anthelmintic activity of *Imperata cylindrica* underground parts. *BMC Complement. Med. Ther.* **20**, 1–9 (2020).
65. Sharma, P. Histochemical studies on the distribution of alkaline phosphatase, acid phosphatase, 5-nucleotidase and ATPase in various reproductive tissues of certain digenetic trematodes. *Z. Parasitenkd.* **49**, 223–231 (1976).
66. Pal, P. & Tandon, V. Anthelmintic efficacy of *Flemingia vestita* (Fabaceae): Genistein-induced alterations in the esterase activity in the cestode. *Raillietina echinobothrida*. *J. Biosci.* **23**, 25–31 (1998).
67. Pearse, A. G. E. *Histochemistry, Theoretical and Applied: Theoretical and Applied* (Churchill Livingstone, 1968).
68. Wachstein, M. & Meisel, E. Histochemistry of hepatic phosphatases at a physiologic pH: With special reference to the demonstration of bile canaliculi. *Am. J. Clin. Pathol.* **27**, 13–23 (1957).

## Acknowledgements
The authors express their heartfelt gratitude to Dr. Debkumar Mukhopadhyay, Vice-Chancellor of CBPBU, for his support and encouragement and for providing the necessary laboratory facilities. The authors are also grateful to the UGC-DAE Consortium, Kolkata, for the XRD facility and Centre for Research in Nanoscience and Nanotechnology, University of Calcutta (CRNN, CU), for allowing us to use their SEM, TEM and FTIR facility.

## Author contributions
R.M. and P.K.K. conceived the idea and designed the research. R.M. performed the experiments, analyzed, and interpreted the data. R.M. and P.K.K. wrote the manuscript. We affirm that all authors read and approved the manuscript and that no other individuals satisfied the authorship requirements but are not included. We further confirm that all have approved the order of the authors listed in the manuscript of us.

## Competing interests
The authors declare no competing interests.

## Additional information
**Supplementary Information** The online version contains supplementary material available at https://doi.org/10.1038/s41598-023-34221-9.

**Correspondence** and requests for materials should be addressed to P.K.K.